Experimental Evaluation of Compressive Behavior of Orthotropic Steel Plates for the New San Francisco–Oakland Bay Bridge

C. C. Chou[1]; C. M. Uang[2]; and F. Seible[3]

Abstract: Compression tests were conducted on two reduced-scale orthotropic plates to verify the design strength of steel box girders for the new San Francisco–Oakland Bay Bridge. The first specimen was composed of three longitudinal closed ribs and a top deck plate. It failed in global buckling, followed by local buckling in the deck plate and ribs. The second specimen, which was composed of four longitudinal T-shaped ribs and a bottom deck plate, experienced global buckling as well as local buckling in the ribs and the deck plate. The ultimate strength and failure mode of both specimens were evaluated by two bridge design specifications: the 1998 AASHTO load and resistance factor design specification and the 2002 Japanese JRA specification. Findings from code comparisons showed that: (1) Sufficient flexural rigidity of ribs were provided for both specimens; (2) the JRA specification slightly overestimated the ultimate strength of both specimens; and (3) neither specifications predicted the observed buckling sequence in Specimen 2. A general-purpose nonlinear finite element analysis program (*ABAQUS*) was used to perform correlation study. The analysis showed that the ultimate strength and postbuckling behavior of the specimens could be reliably predicted when both the effects of residual stresses and initial geometric imperfections were considered in the model.

DOI: 10.1061/(ASCE)1084-0702(2006)11:2(140)

CE Database subject headings: Steel plates; Compression tests; Bridges, cable-stayed; California; San Francisco.

Introduction

The new East Span of the San Francisco–Oakland Bay Bridge (SFOBB), designed by the joint venture of TY Lin International and Moffatt & Nichol, features a 565 m long single tower steel self-anchored suspension bridge with a main span of 385 m (see Fig. 1). The cable is anchored to the deck at the east bent and is looped around at the west bent. The suspenders spaced at 10 m are splayed to the exterior sides of the steel orthotropic box girders, and floor beams are spaced at 5 m inside the box girder. Two box girders, which are interconnected with cross beams at 30 m on center, are in compression in order to balance the cable tension forces. The seismic force demand on the box girders due to a 1,500 year safety evaluation earthquake (SEE) event is large; the demand-to-capacity ratio of the compressive stress at some locations was estimated in design to range from 0.8 to 1.0. Fig. 2 shows three different types of longitudinal ribs (troughs, structural tees, and flat plates) that are used to stiffen the deck plates. Flat plates and structural tees are denoted as open (torsionally soft) ribs, and troughs are denoted as closed (torsionally stiff) ribs, which are more efficient than the former in distributing wheel loads on the top deck plate.

The box girders in the new Bay Bridge can experience one or a combination of the following buckling modes:

1. Overall buckling of the box girder between the main tower and the anchor of the cable;
2. Buckling of the deck plate between floor beams;
3. Buckling of the deck plate between ribs; and
4. Buckling of ribs.

This experimental program focused on the investigation of the compressive strength and postbuckling behavior of stiffened deck plates to ensure that buckling would not occur before the yield

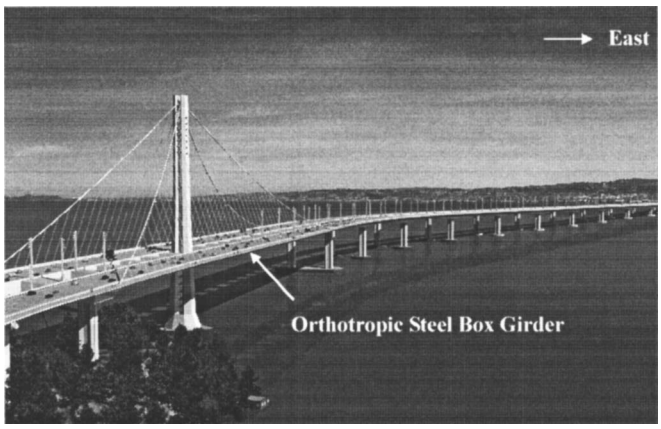

Fig. 1. Bridge elevation

[1]Assistant Professor, Dept. of Civil Engineering, National Chiao Tung Univ., Hsinchu 300, Taiwan (Corresponding author). E-mail: chchou@mail.nctu.edu.tw

[2]Professor, Dept. of Structural Engineering, Univ. of California, San Diego, La Jolla, CA 92093-0085. E-mail: cmu@ucsd.edu

[3]Dean, Jacobs School of Engineering, Univ. of California, San Diego, La Jolla, CA 92093-0085. E-mail: seible@ucsd.edu

Note. Discussion open until August 1, 2006. Separate discussions must be submitted for individual papers. To extend the closing date by one month, a written request must be filed with the ASCE Managing Editor. The manuscript for this paper was submitted for review and possible publication on October 20, 2004; approved on March 3, 2005. This paper is part of the ***Journal of Bridge Engineering***, Vol. 11, No. 2, March 1, 2006. ©ASCE, ISSN 1084-0702/2006/2-140–150/$25.00.

J. Bridge Eng. 2006.11:140-150.

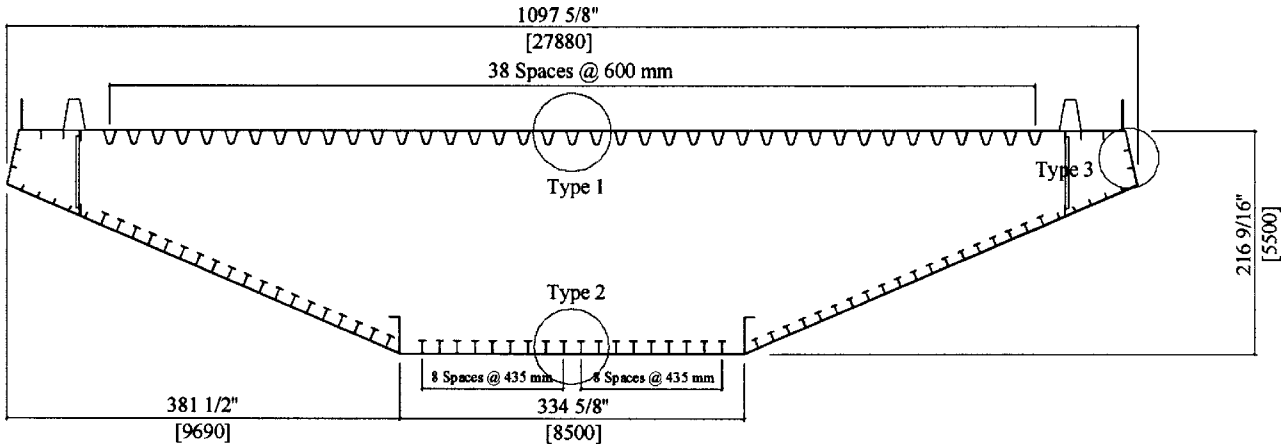

Fig. 2. Prototype orthotropic steel box girder section

capacity of the deck plate was reached. Reduced-scale tests on two orthotropic plates that simulated a portion of the top and bottom decks (see Fig. 2) were conducted. The ultimate strength and the observed failure mode were compared with those predicted by two bridge codes: the AASHTO load and resistance factor design (LRFD) specification (AASHTO 1998) and the Japan Road Association (JRA) specification (JRA 2002). A correlation study using a nonlinear finite element analysis program (*ABAQUS*) was also performed.

Literature Review

Extensive research on the compressive strength of orthotropic plates has been conducted in Europe since early 1970s. These research activities [e.g., Horne and Narayanan (1976) and Moolani and Dowling (1976)] focused mainly on the significance of parameters such as plate and rib geometric imperfections, width–thickness ratio, slenderness ratio, and residual stresses. The testing program conducted at the University of Manchester (Horne and Narayanan 1976) included 52 stiffened plates with different rib types (e.g., flats, bulb flats, angles, and tees) and welding processes. Test results were compared with the Merrison rules (Merrison Committee 1973), which idealize an orthotropic plate as a series of individual struts; each strut is composed of a rib and a plate with a certain width. Comparisons showed that the Merrison predictions for the ultimate strength were conservative for low slenderness and width–thickness ratios and unreliable for high slenderness and width–thickness ratios.

In Japan, stiffened steel plates are used not only in bridge superstructures but also in steel bridge piers. A significant amount of the research (Fukumoto et al. 1974; Hasegawa et al. 1976; Yamada et al. 1978; Watanabe et al. 1981; Nakai et al. 1984; Kitada et al. 1991) was focused on analytical and experimental investigations of the ultimate strength of stiffened plates composed of either open or closed ribs subjected to uniaxial or biaxial compression. Several empirical formulations were proposed to predict the ultimate strength. These studies used the flexural rigidity of ribs as a common parameter, which is useful for rib design. However, the minimum stiffener rigidity does not necessarily give an optimum design (Watanabe et al. 1981).

Grondin et al. (1999, 2002) studied T-shaped stiffened plates under compression. When the effects of residual stresses and geometry imperfections were considered, nonlinear finite element models were found to be able to predict the ultimate strength and postbuckling behavior of the test units. It was reported that overall buckling of the stiffened plates is a preferred failure mode than the buckling of ribs or plates because the postbuckling behavior of the former is more stable.

Galambos (1998) summarized important research work on stiffened plates under compression. The minimum moment of inertia of the T-shaped ribs, required to ensure an antisymmetric buckling mode of the stiffened plates, was investigated by Yoo et al. (2001). Ignoring the effects of residual stress and initial geometric imperfection, results from elastic finite element analyses showed that the required moment of inertia of the ribs in accordance with the AASHTO specifications (AASHTO 1998) is too conservative.

Objectives

The objectives of this study were (1) to verify experimentally the design capacity of the stiffened plates; (2) to examine whether local buckling of longitudinal ribs would occur before global buckling of the stiffened plates; and (3) to evaluate the postbuckling behavior of the stiffened plates for the box girders of the new SFOBB east span. Test results of two scaled specimens were compared with those predicted by two design specifications and finite element analyses.

Test Specimens

The axial load of each specimen was applied vertically by a horizontal loading beam, which was pin connected to a reaction wall at one end (Fig. 3). The compression load was provided by two 2,000 kN actuators at the other end of the loading beam. Pin supports were provided at the top and bottom ends of the specimens. The specimens were also braced laterally at midheight by a diaphragm plate to simulate the floor beam action in the box girder. Such a configuration would allow the effect of buckling direction to be considered in one test. The cross sections of both specimens are shown in Fig. 4. *ASTM A709* Grade 345 (50 ksi) steel was specified; the material characteristics obtained from certified mill test reports are listed in Table 1.

J. Bridge Eng. 2006.11:140-150.

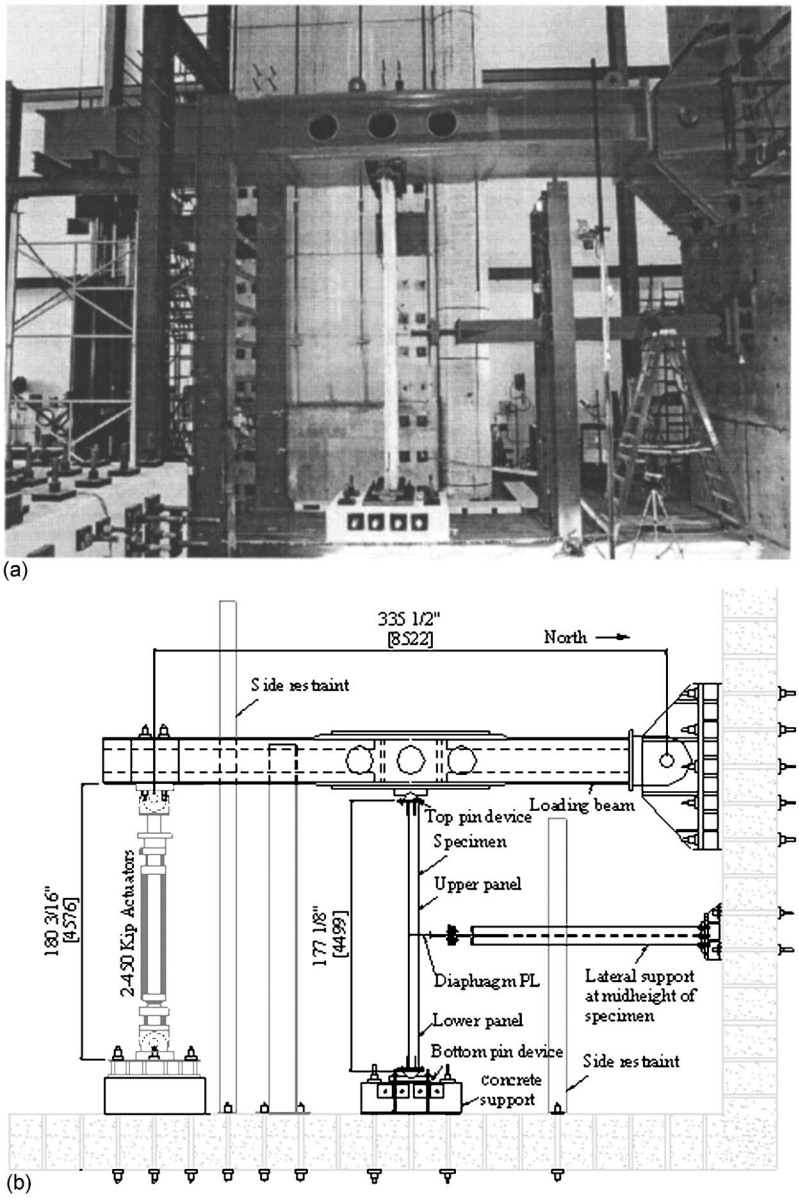

Fig. 3. Global view before testing: (a) Specimen in position; and (b) test setup

Specimen 1, with a scale factor of 0.45, was composed of three closed ribs and a top deck plate. Partial-joint penetration groove welding between the closed ribs and the deck plate was performed by an automated SAW welding process. Specimen 2, with a scale factor of 0.475, was made up of a bottom deck plate and four T-shaped ribs, each of which being built up by a web plate and a flange plate. To avoid localized yielding and buckling, each specimen was strengthened by stiffeners at loading ends. Sectional properties for both actual and target models are listed in Table 2.

Because each specimen was located at the midspan of the loading beam, the compression force is twice the actuator forces. The axial deformation (Δ) of the specimen was computed as the average of two measurements made by a pair of displacement transducers placed along both edges of the specimen. In this paper, positive bending direction is defined as the bending about which the deck plate of the specimen is in compression. The upper panel is defined as the portion of the specimen above the midheight.

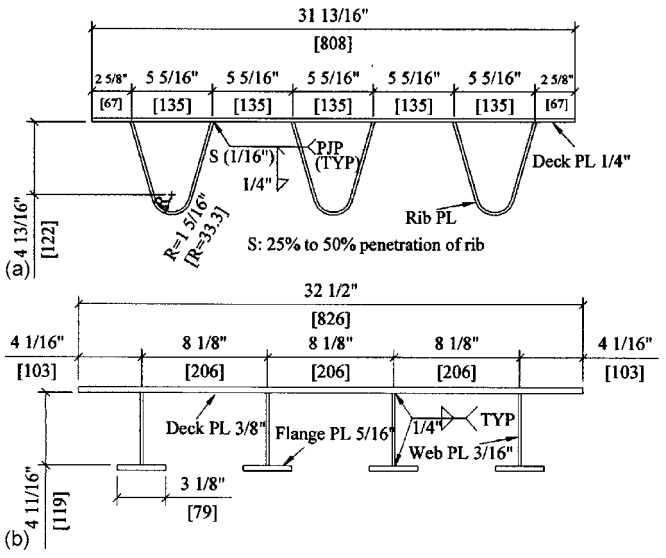

Fig. 4. Specimen cross sections: (a) Specimen 1; and (b) Specimen 2

J. Bridge Eng. 2006.11:140-150.

Table 1. Specimen Material Properties

Specimen number	Plate	Thickness [mm (in.)]	Yield strength [MPa (ksi)]	Tensile strength [MPa (ksi)]	Elongation[a] (%)
1	Deck plate	6 (0.25)	372 (54)	510 (74)	20
	Rib plate	5 (0.19)	427 (62)	579 (84)	20
2	Deck plate	10 (0.38)	427 (62)	534 (78)	24
	Rib web plate	5 (0.19)	427 (62)	579 (84)	20
	Rib flange plate	8 (0.31)	476 (69)	573 (83)	21

[a]Based on 203 mm (8 in.) gauge length.

Test Results

Specimen 1

The applied load versus axial deformation relationship of Specimen 1 is shown in Fig. 5(a). The maximum strength, 371 MPa (54 ksi), was reached at $\Delta=14$ mm (0.55 in.) with the specimen buckled in reverse curvature [Fig. 6(a)]. Fig. 7(a) shows the strain profiles across the width of the deck plate at the midheight of the upper panel, indicating that the full width of the deck plate was effective in resisting the compression load. The functional evaluation earthquake (FEE) and SEE force demands are marked. As the imposed axial deformation was increased further, local buckling of the ribs in the lower panel and the deck plate in the upper panel was observed at $\Delta=17$ mm (0.68 in.) and 23 mm (0.90 in.), respectively. The symmetric, bulging configuration of the buckled ribs in Fig. 8(b) was compatible in deformation with the buckling pattern of the deck plate schematically graphed in Fig. 9(a). Fig. 8(c) shows the buckling of the ribs that occurred near the upper end of the lower panel; note that the deck plate did not buckle. Also note that the configuration of the buckled rib is different from that shown in Fig. 8(b) for the upper panel. The difference was primarily caused by the direction of bending [Fig. 8(a)] after the maximum strength of the specimen was reached (Chou et al. 2003).

Specimen 2

The applied load versus axial deformation relationship of Specimen 2 is shown in Fig. 5(b), in which the ultimate compression strength, 417 MPa (60 ksi), was reached at $\Delta=17$ mm (0.64 in.). The specimen also buckled in reverse curvature [Fig. 6(b)]. Fig. 7(b) shows the strain profiles across the width of the deck plate at the midheight of the upper panel, which indicates that the full width of the deck plate was also effective in carrying the compression load. Buckling of the T-shaped ribs, similar to a torsional type of buckling mode, was observed in the lower panel [Fig. 10(a)], but not in the upper panel [Fig. 10(b)]. This buckling mode was initiated by the particular (i.e., negative) bending direction, which introduced additional compressive stress in the lower-panel ribs. The buckling of these T-shaped ribs caused the lower panel to twist at $\Delta=20$ mm (0.8 in.). Such a phenomenon was not observed in the upper panel. Instead, local buckling of the deck plate with the ribs forming the nodal lines was observed at 28 mm (1.1 in.) [Fig. 9(b)]. Fig. 11 shows twisting of the lower panel, local buckling of the upper-panel deck plate, and buckling of the ribs in the lower panel.

Strength Correlation with Code Provisions

The measured strengths and buckling modes of the test specimens were compared with those predicted by the following specifications: (1) AASHTO-LRFD bridge design specification (AASHTO 1998), and (2) Japanese design specification (JRA 2002). To compute the compressive strength, a stiffened plate is treated as a series of disconnected struts; each strut consists of one longitudinal rib and a tributary width of the deck plate.

AASHTO-LRFD Bridge Design Specification (AASHTO 1998)

Section 6.14.3.3.3 stipulates that the strut be designed as a compressive member simply supported between floor beams, while local buckling strength may be evaluated by using the formulas in Appendix II of the *Design Manual for Orthotropic Steel Plate Deck Bridges* (Wolchuk 1963). The elastic buckling stress of a simply supported strut is

$$F_i = \frac{\pi^2 E}{\left(\frac{L}{r}\right)^2} \tag{1}$$

where L, r, and E=length of the specimen, radius of gyration about the axis of bending, and modulus of elasticity. When the

Table 2. Sectional Properties for Target and Actual Models

Scale	A (mm^2)	I (mm^4)	r (mm)	L (mm)	L/r	W/t_g	d_{c2}/t_c	$b_f/2t_f$	d_w/t_w
(a) Specimen 1									
Target	10,791	32,704,184	55.1	2,250	40.8	21.4	25.1	—	—
Actual	10,174	30,604,664	54.8	2,249	41.0	21.3	28.7	—	—
Ratio	0.94	0.94	0.99	1.00	1.00	1.00	1.14	—	—
(b) Specimen 2									
Target	12,725	36,253,520	53.4	2,375	44.5	21.8	—	5.0	24.4
Actual	12,645	35,995,334	53.4	2,369	44.4	21.7	—	5.0	25.0
Ratio	1.01	1.01	1.00	1.00	1.00	1.00	—	1.00	0.98

J. Bridge Eng. 2006.11:140-150.

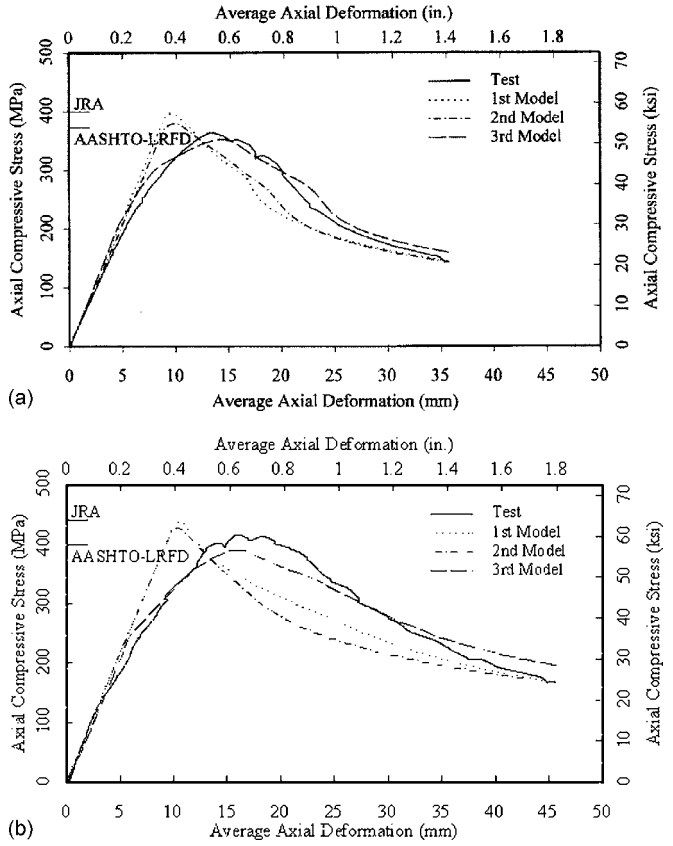

Fig. 5. Applied load versus axial deformation relationships: (a) Specimen 1; and (b) Specimen 2

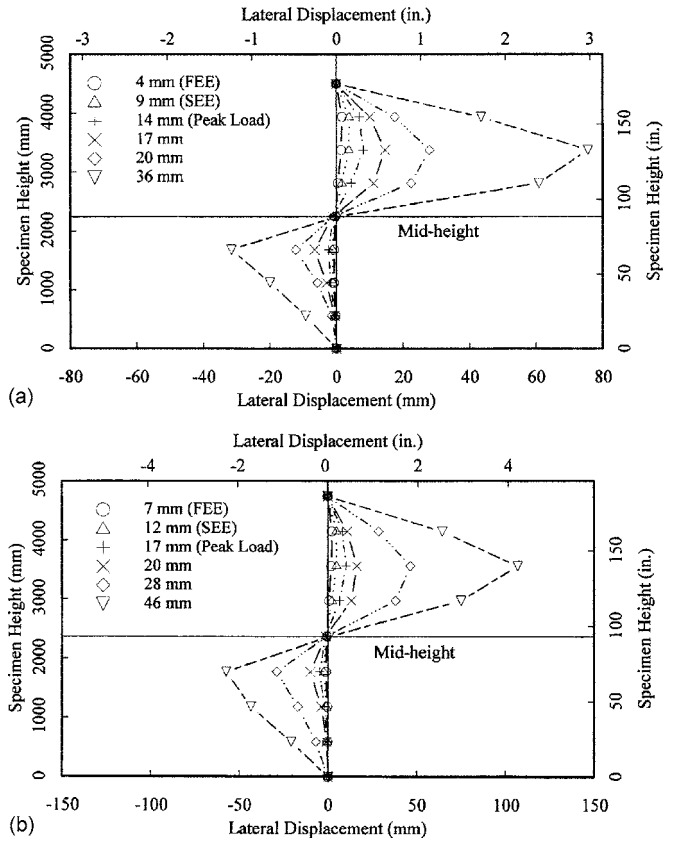

Fig. 6. Laterally deflected profiles along specimen height: (a) Specimen 1; and (b) Specimen 2

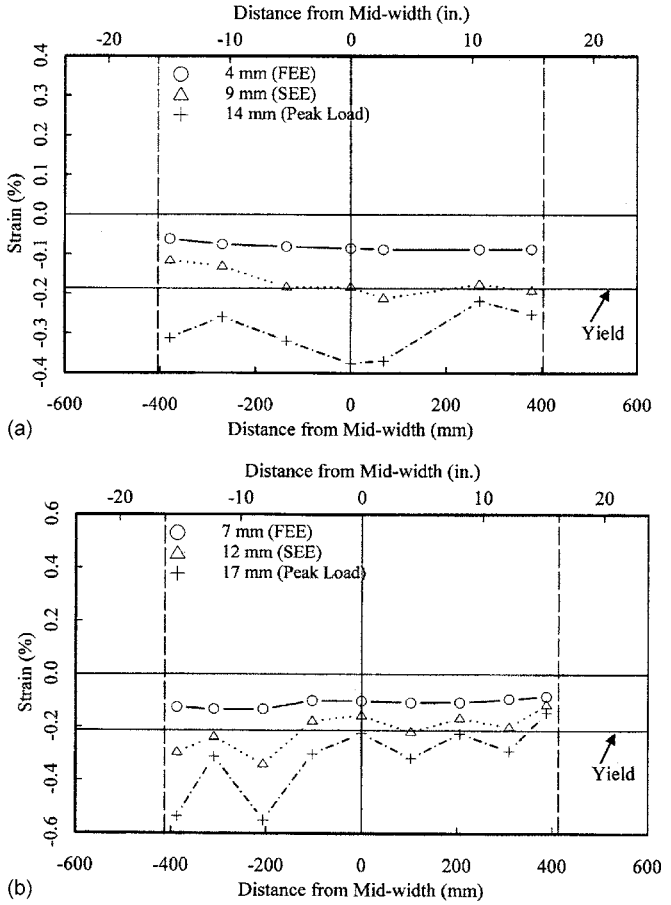

Fig. 7. Longitudinal strain profiles across deck plate width (upper panel): (a) Specimen 1; and (b) Specimen 2

elastic buckling stress exceeds the proportional limit stress (=75% of the yield stress, F_y), the inelastic buckling stress, F_u, of the strut is computed as.

$$\frac{F_u}{F_y} = 1 - 0.1875\frac{F_y}{F_i} \tag{2}$$

To evaluate the local buckling strength, the cross section of the strut is divided into several components. Fig. 12 shows the dimensions and boundary conditions of each component; see Table 3 for the associated buckling coefficient k values for Eq. (3). The elastic buckling stress, F_i, of a plate simply supported at loading edges is given by

$$F_i = k\frac{\pi^2 E}{12(1-\nu^2)}\left(\frac{t}{d}\right)^2 \tag{3}$$

where k, t, d, and ν=buckling coefficient, plate thickness, plate depth, and Poisson's ratio. When the stress in Eq. (3) exceeds the proportional limit stress, the inelastic buckling stress, F_u, is computed as (Wolchuk 1963)

$$\frac{F_u}{F_y} = \frac{1}{1 + 0.1875\left(\frac{F_y}{F_i}\right)^2} \tag{4}$$

Based on the above procedure, the calculated stresses for both local and global buckling modes are summarized in Table 4. Since the yield strengths of the deck and rib plates are different, for global buckling the average yield strength, computed as the

J. Bridge Eng. 2006.11:140-150.

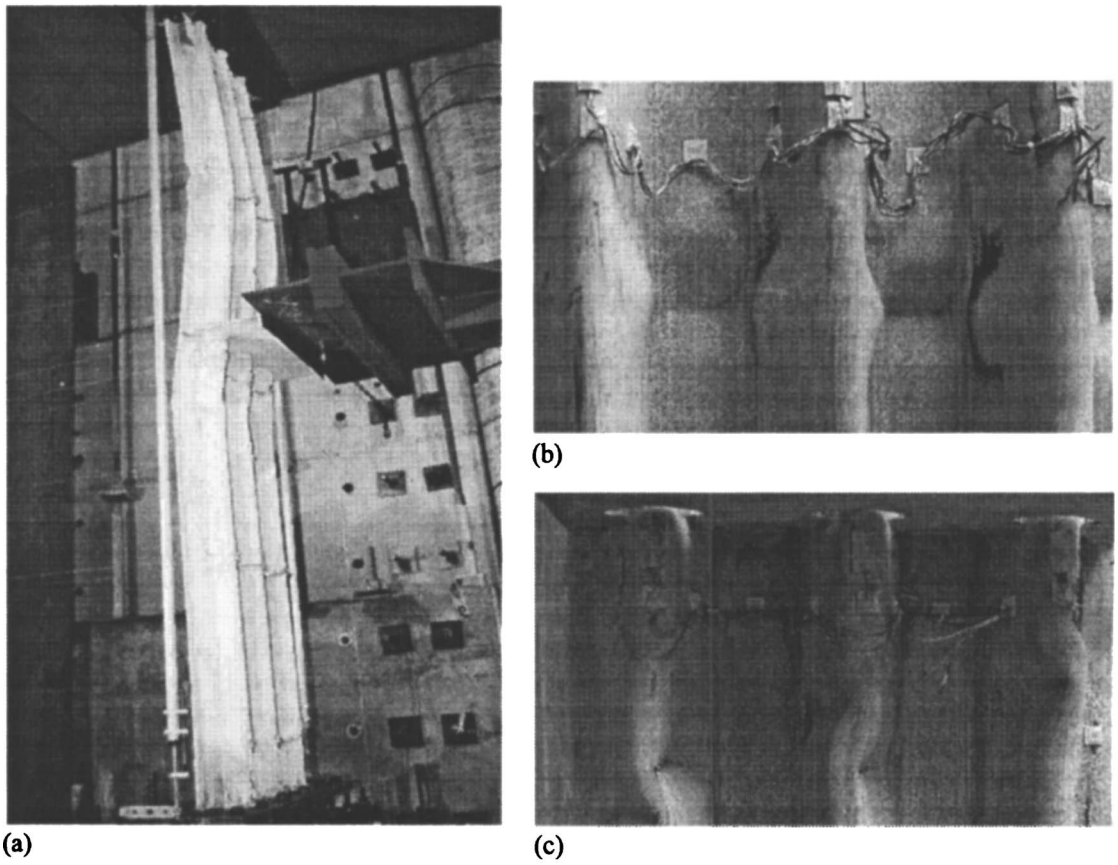

Fig. 8. Deformed configurations after testing (Specimen 1): (a) Overall view; (b) upper panel; and (c) lower panel

yield capacity divided by the total area (Table 5), was used. The calculations predicted that for Specimen 1 global buckling and local buckling of the deck plate occurred almost at the same time, and that Specimen 2 buckled globally first, which was followed by local buckling of the web plate, causing twist of the T-shaped ribs.

Japanese Design Specification

Sections 8.4.4–8.4.6 of the JRA specification (JRA 2002) specifies the minimum thickness of the prototype deck plate and closed ribs (U-shaped type) to be 12 and 6 mm, respectively, which corresponded to a width–thickness ratio of 27 and 40 for the deck and rib plates, respectively. The width–thickness ratios of Specimen 1 in Table 6 indicate that this compactness requirement is satisfied. Therefore, the compressive strength can reach the yield strength.

According to Sections 4.2.4 and 4.2.5 of the JRA, the ultimate strength of a uniformly compressed plate stiffened with open ribs (T-shaped type) is computed as follows:

$$\frac{F_u}{F_y} = \begin{Bmatrix} 1.0 & R \leq 0.5 \\ 1.5 - R & 0.5 < R \leq 1.0 \\ 0.5/R^2 & R > 1.0 \end{Bmatrix} \tag{5}$$

where

$$R = \frac{b}{t}\sqrt{\frac{F_y}{E}\frac{12(1-\nu^2)}{\pi^2 k}} \tag{6}$$

The buckling coefficient, k, is a function of the number of subpanels, n, the aspect ratio, α, the area ratio of one rib to the deck plate, δ, and the flexural rigidity ratio of one rib to the deck plate, γ_l. The calculated values of k and R in Table 7 indicate that the yield strength can be reached. Also, a comparison of the moment of inertia of the rib (I_r) with that required ($I_{\min}$) by the JRA

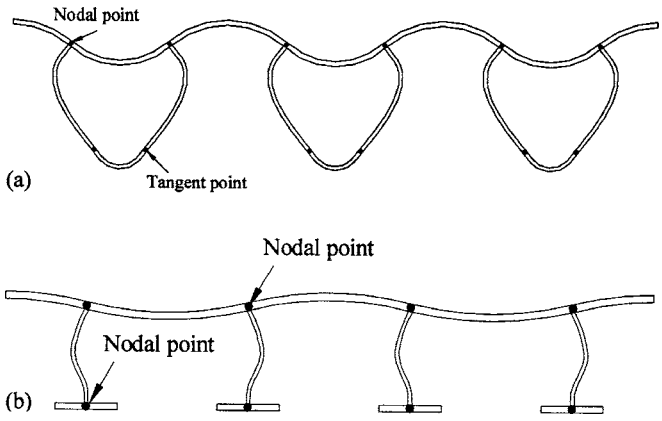

Fig. 9. Schematic buckling configurations at midheight of upper panel: (a) Specimen 1; and (b) Specimen 2

J. Bridge Eng. 2006.11:140-150.

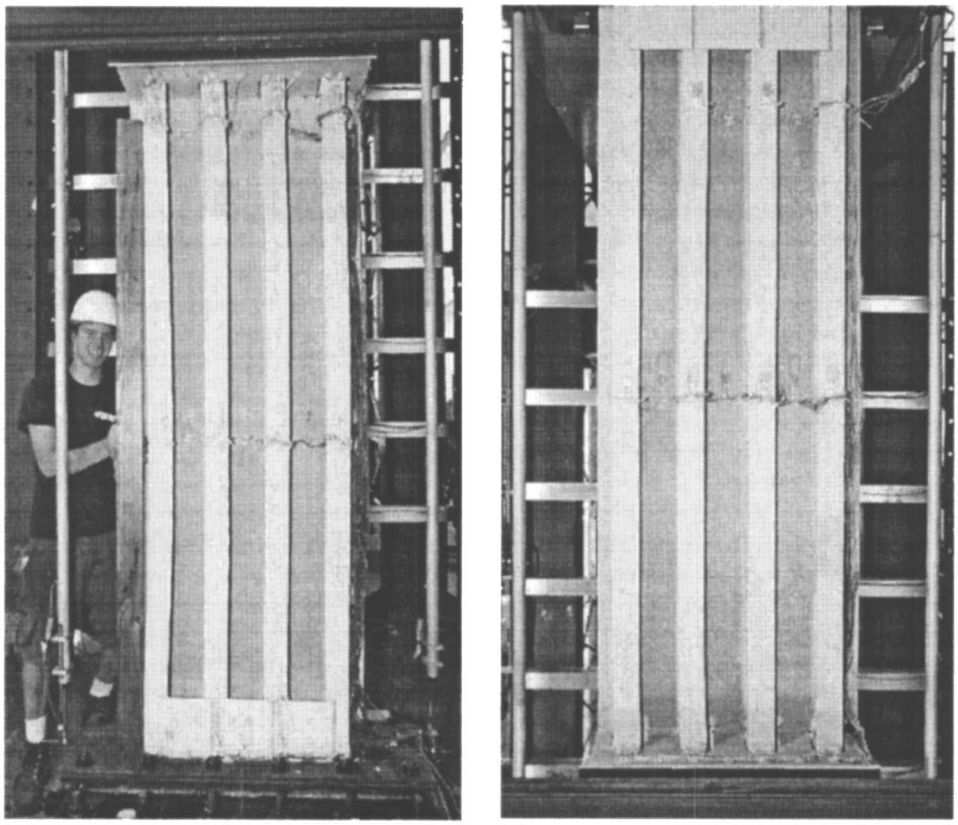

Fig. 10. Deformed configurations at peak strength level (Specimen 2): (a) Lower panel; and (b) upper panel

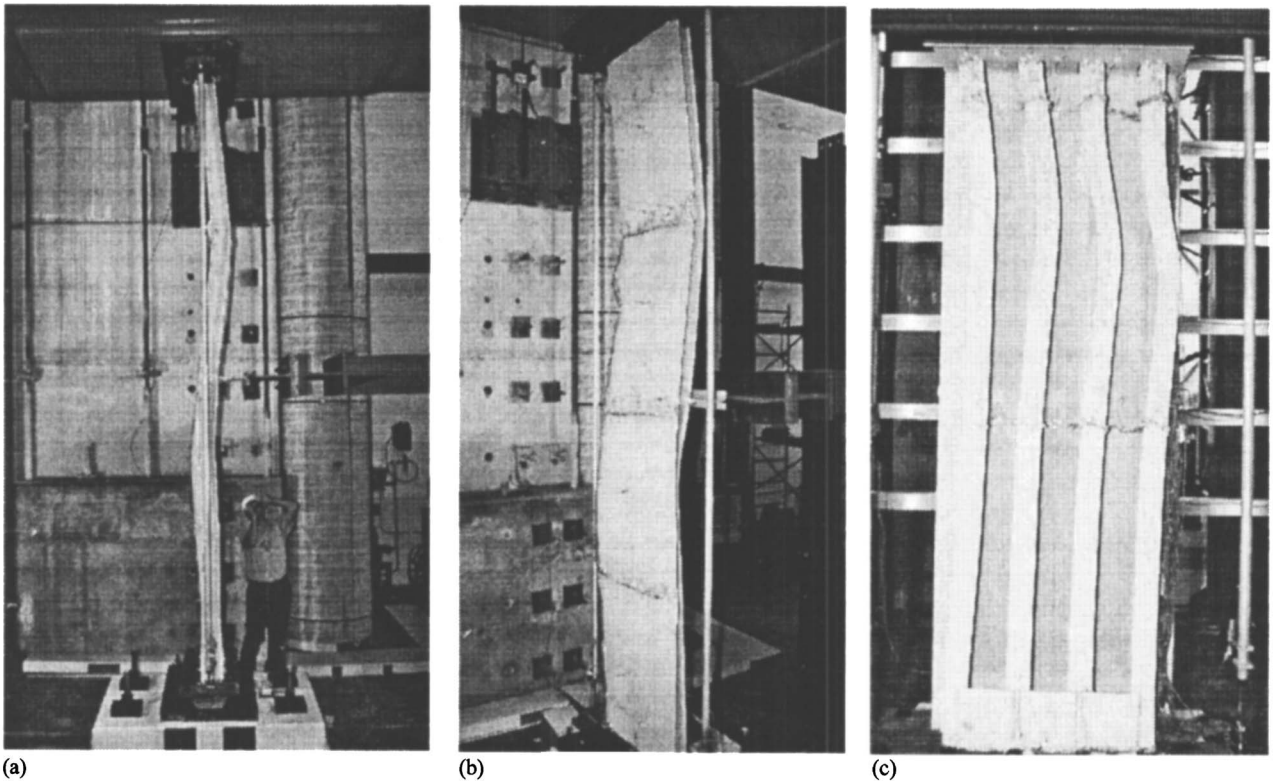

Fig. 11. Deformed configurations after testing (Specimen 2): (a) Side view; (b) front view; and (c) lower panel

J. Bridge Eng. 2006.11:140-150.

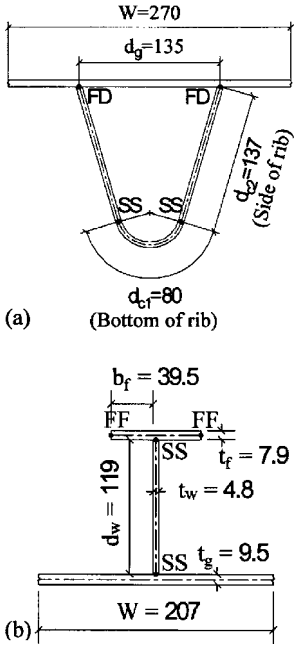

Fig. 12. Dimensions and boundary conditions of strut component: (a) Specimen 1; and (b) Specimen 2

specification indicates that the ribs have sufficient stiffness to force the deck plate buckling to occur between ribs.

The predicted strengths based on the two specifications are marked in Fig. 5. For Specimen 1, the JRA specification predicted that the yield strength could be reached. But the measured ultimate strength is better predicted by AASHTO-LRFD. This specification also predicted that global buckling and local buckling of the deck plate [Table 4] occurred almost simultaneously; this prediction is close to the observed buckling sequence.

The JRA specification also overestimated the capacity of Specimen 2. The predicted strength of AASHTO-LRFD is slightly conservative. Both specifications predicted that global buckling, not local buckling, would occur first.

Finite Element Analysis

Both test specimens were modeled with the nonlinear finite element computer program *ABAQUS* (HKS 2001); the four-node doubly curved thin shell element S4R was used. Because the initial geometric imperfections and residual stresses have

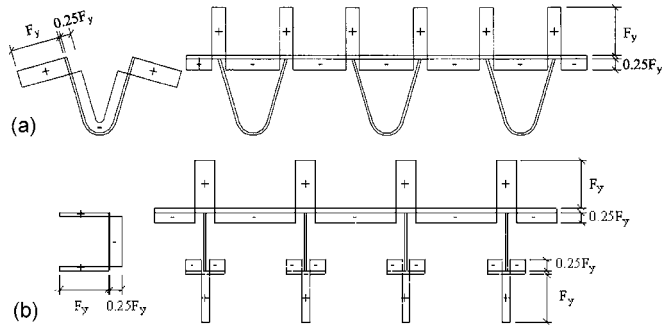

Fig. 13. Assumed residual stress distribution pattern (positive for tensile stress): (a) Specimen 1; and (b) Specimen 2

Table 3. Values of k for Different Edge Conditions

Edge conditions				
FD-FD	FD-SS	SS-SS	FD-FF	SS-FF
6.97	5.40	4.00	1.28	0.43

Note: FD=fixed edge; SS=simply supported edge; and FF=free edge.

Table 4. Predicted Compressive Strength per AASHTO-LRFD

	Local buckling rib plate (side)	Local buckling rib plate (bottom)	Local buckling deck plate	Global buckling
Specimen 1				
d (mm)	137	80	135	
t (mm)	5	5	6	L/r=41
k	5.4	4.0	6.97	A=10,174 mm^2
F_y (MPa)	427	427	372	400
F_i (MPa)	1,200	2,599	2,786	1,172
F_u (MPa)	417	425	371	372
	Local buckling flange plate	Local buckling web plate	Local buckling deck plate	Global buckling
Specimen 2				
d (mm)	40	119	207	
t (mm)	8	5	10	L/r=44
k	0.43	4	4	A=12,645 mm^2
F_y (MPa)	476	427	427	437
F_i (MPa)	3,109	1,179	1,537	1,000
F_u (MPa)	474	417	421	401

Table 5. Specimen Yield Capacity Based on Measured Yield Strength

Specimen number	Element	Section area [mm^2 (in.^{2})]	Yield capacity [kN (kips)]
1	Deck plate	5,151 (8.0)	1,922 (432)
	Rib plate	5,023 (7.8)	2,154 (484)
	Σ	10,174 (15.8)	4,076 (916)
2	Deck plate	7,871 (12.2)	3,364 (756)
	Web plate	2,258 (3.5)	966 (217)
	Flange plate	2,516 (3.9)	1,197 (269)
	Σ	12,645 (19.6)	5,527 (1,242)

Table 6. Width–Thickness Ratios of Specimen 1 per JRA (2002)

Element	Width/thickness ratio
Deck plate	21
Rib (side)	27
Rib (bottom)	16

Table 7. Characteristic Values for Specimen 2 per JRA (2002)

n	α	δ	γ_l	k	I_r/I_{min}	R
5	2.9	0.15	188	71	1.16	0.45

J. Bridge Eng. 2006.11:140-150.

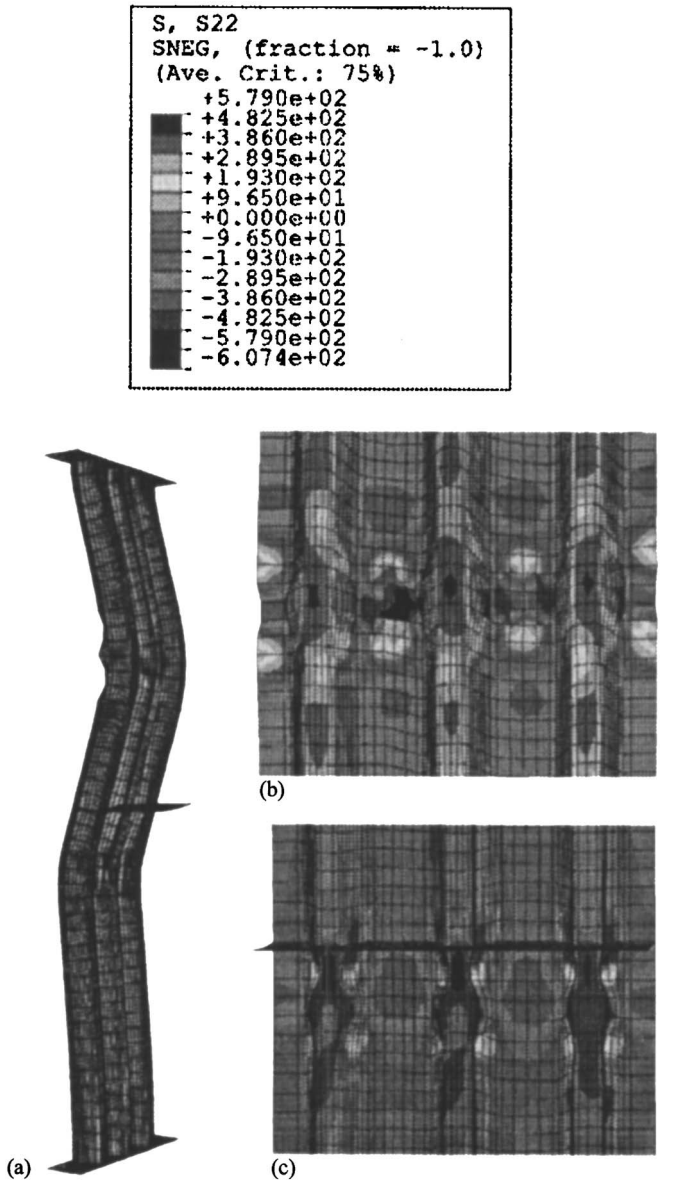

Fig. 14. Predicted deformed geometry of Specimen 1: (a) Overall deformation; (b) upper panel; and (c) lower panel

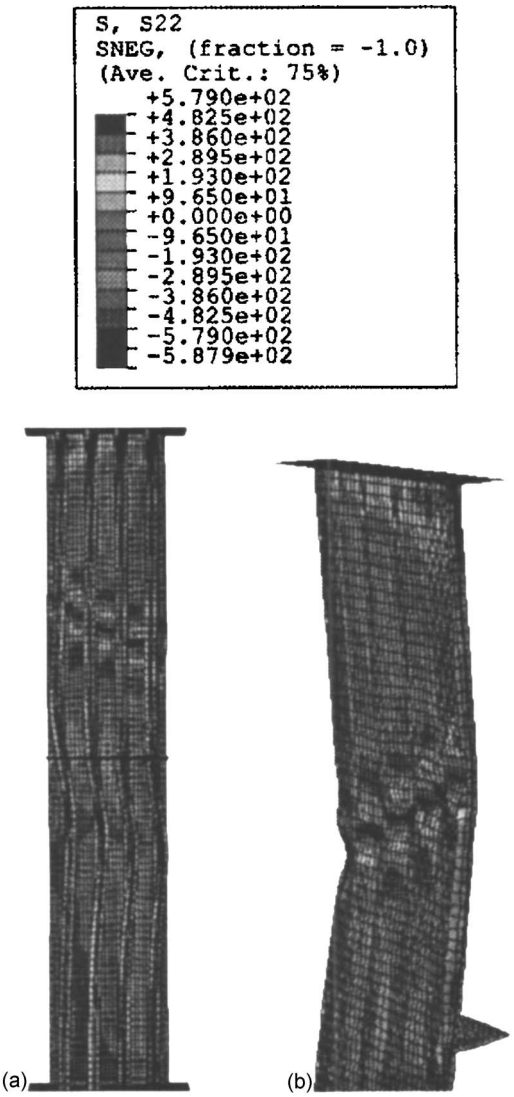

Fig. 15. Predicted deformed geometry of Specimen 2: (a) Overall deformation; and (b) view from deck plate side

pronounced influences on the ultimate strength and postbuckling behavior of the stiffened plates (Fukumoto et al. 1974; Grondin et al. 2002), these two effects were considered in this study. Since the residual stresses of the fabricated specimens were not measured, the patterns of residual stresses suggested by Fukumoto et al. (1974) and Grondin et al. (2002) were assumed (Fig. 13). The residual stresses were introduced in the model by defining initial stresses across the thickness of shell elements. The measured geometric imperfections between the center and the end of the respective deck plate were about 9 and 6 mm for Specimens 1 and 2, respectively, which were less than the tolerance limits of 11 and 9 mm, calculated based on Section 11.4.13.2 of the *Standard Specifications for Highway Bridges* (AASHTO 2002)

$$\frac{b}{26\sqrt{t_g}} \tag{7}$$

where b=width of the deck plate and t_g=deck plate thickness. The measured geometric imperfection of each specimen was approximated by applying a uniform pressure perpendicular to the deck plate to mimic the deformed pattern and the magnitude.

Three models were considered for each test specimen. Ignoring the effects of both geometric imperfections and residual stresses in the first model, the ideal yield capacity of the specimen could be reached before strength degradation (see Fig. 5). By considering only the initial geometric imperfections in the second model, the predicted ultimate strength and elastic stiffness were slightly lower than those of the first model, but were higher than the test results. When both effects were considered in the third model, the predicted response correlated well with the peak strength and the postbuckling behavior (Fig. 5). Numerical simulation from the second and third models showed that the effect of residual stresses is more significant than that of geometric imperfections in the buckling behavior.

The predicted buckling modes were similar to those observed in the tests (Figs. 14 and 15). Different local buckling modes in the rib plate due to the effect of bending direction were predicted in Specimen 1 [see Figs. 14(b and c)]. For Specimen 2, twisting of the T-shaped ribs in the lower panel and local buckling of the deck plate in the upper panel were also predicted [see Figs. 15(a and b)].

J. Bridge Eng. 2006.11:140-150.

Conclusions

Two reduced-scale, longitudinally stiffened plates that simulate a portion of the top and bottom deck plates of the steel box girders for the east span of the New San Francisco–Oakland Bay Bridge were tested to evaluate the compressive strength and postbuckling behavior. The first specimen incorporated a top deck plate and three closed ribs (troughs), while the second specimen incorporated a bottom deck plate and four open T-shaped ribs. To evaluate the effect of buckling direction in the test, each specimen featured a two-span configuration with the midspan supported laterally to simulate the floor beam effect.

The compression test results showed that the deck plate of both specimens could reach yield before local buckling occurred. For Specimen 1, the strength degradation was due to global buckling, local buckling of the closed ribs in one span, and local buckling of the deck plate in another span; the different local buckling modes observed in each span reflect the effect of bending (or buckling) direction. For Specimen 2, the strength degradation was caused by buckling of the T-shaped ribs in one span and local buckling of the deck plate in another span.

The ultimate strengths of both specimens were compared with those predicted by two design specifications. The JRA specification tended to overestimate the strength. The AASHTO-LRFD specification provided a better estimate of the strength. Although this specification also predicted the buckling mode of Specimen 1, neither it nor the JRA specification predicted the observed buckling sequence in Specimen 2.

Correlation study using a nonlinear finite element analysis program *(ABAQUS)* confirmed that a reliable prediction of the ultimate strength and postbuckling behavior requires that the effects of both residual stresses and geometric imperfections be considered. Numerical simulation also showed that the effect of residual stresses is more significant than that of geometric imperfections considered in this study.

Acknowledgments

This research project was sponsored by the California Department of Transportation (Caltrans). The tests were conducted in the Charles Lee Powell Structural Laboratories at UCSD; Dr. Wenyi Long and Mr. Francisco Carpio from Caltrans and Dr. Marwan Nader and Mr. Laurent Rus from TY Lin International provided invaluable assistance to this testing program.

Notation

The following symbols are used in this paper:

A = area of specimen;
A_r = area of rib;
b = deck plate width;
b_f = flange plate width;
d = Plate depth;
d_{c1} = length of bottom of closed rib;
d_{c2} = length of side of closed rib;
d_g = spacing between side of closed rib on deck plate;
d_w = length of web plate;
E = modulus of elasticity;
F_i = elastic buckling stress;
F_P = stress proportional limit;
F_u = inelastic buckling stress;
F_y = yield stress;
I = moment of inertia of section about centroid axis parallel to plate;
I_r = moment of inertia of rib about axis parallel to plate surface at base of rib;
$I_{\min}$ = required moment of inertia of rib;
k = buckling coefficient;
L = specimen length between hinge supports;
n = number of subpanels;
r = radius of gyration about axis of buckling;
t = plate thickness;
t_c = closed rib thickness;
t_f = flange plate thickness;
t_g = deck plate thickness;
t_w = web plate thickness;
W = rib spacing,
α = aspect ratio;
γ_l = ratio of flexural stiffness between rib and deck plate;
Δ = axial deformation;
δ = ratio of rib area to deck plate area; and
ν = Poisson's ratio.

References

American Association of State Highway and Transportation Officials (AASHTO). (1998). *LRFD bridge design specifications*, AASHTO, Washington, D.C.

American Association of State Highway and Transportation Officials (AASHTO). (2002).*Standard specifications for highway bridges*, AASHTO, Washington, D.C.

Chou, C. C., Uang, C. M., and Seible, F. (2003). "Compression testing of orthotropic steel deck for the new San Francisco–Oakland bay self-anchored suspension bridge." *Rep. No. SSRP-2002/12*, Dept. of Structural Engineering, Univ. of California, San Diego, La Jolla, Calif.

Fukumoto, Y., Usami, T., and Okamoto, Y. (1974). "Ultimate compressive strength of stiffened plates." *Proc., Specialty Conf. on Metal Bridge*, St. Louis, Mo.

Galambos, T. V. (1998). *Structural stability design criteria for metal structures*, Wiley, New York.

Grondin, G. Y., Elwi, A. E., and Cheng, J. J. R. (1999). "Buckling of stiffened steel plates—A parametric study." *J. Constr. Steel Res.*, 50, 151–175.

Grondin, G. Y., Wang, E., and Elwi, A. E. (2002). "Interaction buckling of stiffened steel plates." *Proc., Structural Stability Research Council Annual Technical Session*, Structural Stability Research Council, Washington, D.C.

Hasegawa, A., Ota, K., and Nishino, F. (1976). "Buckling strength of multiple stiffened plates." *Methods of structural analysis*, W. E. Saul, and A. H. Peyrot, eds., *Proc., National Structural Engineering Conf.*, Vol. 2, Madison, Wis., 937–956.

Hibbitt, Karlsson, & Sorensen (HKS). (2001). *ABAQUS user's manual, Version 6.2*, Hibbitt, Karlsson, & Sorensen, Inc., Pawtucket, R.I.

Horne, M. R., and Narayanan, R. (1976). "Ultimate strength of stiffened panels under uniaxial compression." *Steel plated structures*, P. J. Dowling, J. E. Harding, and P. A. Frieze, eds., Crosby Lockwood, London.

Japan Road Association (JRA). (2002). *Specification for highway bridges: Part I*, JRA, Tokyo.

Kitada, T., Nakai, H., and Furuta, T. (1991). "Experimental study on ultimate strength of stiffened plates subjected longitudinal tension and transverse compression." *J. Constr. Steel Res.*, 19, 203–212.

Merrison Committee. (1973). "Interim design and workmanship rules,

committee of inquiry into the basis of design and method of erection of steel box girders."Merrison Committee, London.
Moolani, F. M., and Dowling, P. J. (1976). "Ultimate load behavior of stiffened plates in compression." *Steel plated structures*, P. J. Dowling, J. E. Harding, and P. A. Frieze, eds., Crosby Lockwood, London, 51–88.
Nakai, H., Kitada, T., and Taido, Y. (1984). "A design method of wide stiffened plates subjected to compression—Application to design of shallow box girder in long span cable-stayed bridge over river at Osaka Bay, Japan." Osaka City Univ., Osaka, Japan.
Watanabe, E., Usami, T., and Hasegawa, A. (1981). "Strength and design of steel stiffened plates—A literature review of Japanese contributions." *Proc., U.S.–Japan Joint Seminar*, Tokyo.
Wolchuk, R. (1963). *Design manual for orthotropic steel plate deck bridges*, American Institute of Steel Construction, Chicago.
Yamada, Y., Watanabe, E., and Ito, R. (1978). "Compressive strength of plates with closed-sectional ribs." *Proc., JSCE*, 133–148.
Yoo, C. H., Choi, B. H., and Ford, E. M. (2001). "Stiffness requirements for longitudinally stiffened box-girder flanges." *J. Struct. Eng.*, 127(6), 705–711.

J. Bridge Eng. 2006.11:140-150.